Published in final edited form as:
Nat Chem. 2011 March ; 3(3): 230–235. doi:10.1038/nchem.982.

DNA Charge Transport over 34 nm

Jason D. Slinker, **Natalie B. Muren**, **Sara E. Renfrew**, and **Jacqueline K. Barton***
Division of Chemistry and Chemical Engineering, California Institute of Technology, Pasadena, California, 91125

Abstract

Molecular wires show promise in nanoscale electronics but the synthesis of uniform, long conductive molecules is a significant challenge. DNA of precise length, by contrast, is easily synthesized, but its conductivity has not been explored over the distances required for nanoscale devices. Here we demonstrate DNA charge transport (CT) over 34 nm in 100-mer monolayers on gold. Multiplexed gold electrodes modified with 100-mer DNA yield sizable electrochemical signals from a distal, covalent Nile Blue redox probe. Significant signal attenuation upon incorporation of a single base pair mismatch demonstrates that CT is DNA-mediated. Efficient cleavage of these 100-mers by a restriction enzyme indicates that the DNA adopts a native conformation that is accessible to protein binding. Similar electron transfer rates are measured through 100-mer and 17-mer monolayers, consistent with rate-limiting electron tunneling through the saturated carbon linker. This DNA-mediated CT distance of 34 nm surpasses most reports of molecular wires.

Charge transport (CT) through conjugated molecules has been the focus of extensive research in an effort to use these molecules as components in the construction of nanoscale circuits[1,2]. Molecular wires provide a unique opportunity to study CT in one and two dimensions and are promising materials for electronic applications such as optoelectronics, energy storage devices, logic circuits, and sensors[3]. Thus, many efforts have been directed toward the fabrication of long, linear conjugated molecules for these purposes[1–9]. However, the synthesis of functional molecular wires is challenging, as these wires must have precisely defined, uniform lengths and functionalized terminal groups to bond to electrodes or electroactive moieties. These requirements have limited the effective length of these conjugated molecules to ~10–20 nm[1–9]. Alternatively, DNA easily satisfies the synthetic requirements of molecular wires[2,10–11]. Unlike other conjugated bridges and molecular monolayer assemblies, DNA synthesis has been mastered to the point of automation. Because of its unique structure and directionality, modification of both the 3′ and 5′ DNA termini can be executed selectively and with high yield to endow DNA with a variety of functionalities. Reaction products may be characterized precisely using mass spectrometry, measurements of melting behavior, and spectroscopy.

The challenge surrounding the use of DNA as a molecular wire, by contrast, arises not in the synthesis, but in obtaining consistent electrical properties from DNA. A wide range of

*Correspondence should be addressed to jkbarton@caltech.edu.

Author Contributions
J.K.B., J.D.S. and N.B.M. conceived and designed the experiments. J.D.S., N.B.M. and S.E.R. executed the experiments. J.D.S., N.B.M. and J.K.B. analyzed the results and co-wrote the paper.

Additional information
Supporting information is available.

There are no competing financial interests.

conductivities has been reported, from insulating to superconducting12–22. However, for those studies that have utilized well characterized connections to the DNA and have preserved the duplex conformation in buffered solution without damaging the bases, high conductivities have been consistently achieved14,19–22. In our own laboratory, we have recently measured single molecule conductivities for 15-mer DNA duplexes bridging a carbon nanotube gap, and we observed resistances through the stacked DNA bases comparable to that expected perpendicular to graphite planes19. Also, in these experiments, attenuation in conductivity was seen in duplexes containing a single base pair mismatch as expected from photophysical studies23. These studies and work by other groups have now established that well-ordered, fully base-paired DNA facilitates electronic CT through the DNA π-stack19–30.

Beyond the basic questions of conductivity, achieving long-range CT in DNA is particularly attractive due to its inherent biological recognition capabilities10,11 and its unmatched capacity to be patterned into precise, nanoscale shapes31,32, ideal for nanoelectronics such as integrated circuits and sensors. The characterization of factors governing DNA conductivity on increasing length scales would not only facilitate the incorporation of DNA into complex nanoscale devices but also its utilization for applications in biotechnology. Solution-based photooxidation studies have shown long range oxidative DNA damage through DNA CT over 20 nm26. DNA electrochemistry provides a direct measure of ground state CT through a well-ordered molecular assembly and is of greater utility for electrical device applications.10,33 However, efficient DNA CT through molecular assemblies has not been demonstrated over long distances, and electrochemical observation of DNA CT has typically been limited to a range of 5 nm (15 base pairs)10. Here we probe CT through 34 nm DNA monolayers (100 base pairs) electrochemically.

RESULTS

Preparation of DNA monolayers

Figure 1 shows the various lengths and features of double stranded DNA used in monolayers for DNA electrochemistry. To make the 100-mer, five single stranded oligonucleotides were synthesized and purified34. Duplexes were prepared by annealing a 27-mer strand with a six-carbon thiol linker at its 5′ terminus and a 73-mer strand to complementary strands including a 39-mer, a 36-mer, and a 25-mer with a Nile Blue redox probe covalently attached through a uracil at its 5′ terminus, which was synthesized as described previously (see Supporting Figure 1)34,36. This piecewise synthesis, involving assembly of the double stranded 100-mer from these overlapping single stranded DNA segments, was employed to improve synthetic yield. Although duplexes prepared in this manner contain nicks in the sugar-phosphate backbone, DNA-mediated CT occurs through the π-stack and not through the backbone35, so these duplexes remain fully functional for DNA CT. The fully assembled 100-mer duplexes were designed such that the Nile Blue redox probe would be positioned at one 5′ terminus of the duplex and the thiol linker would extend from the other 5′ end. To investigate restriction enzyme activity, 100-mers were designed with the *Rsa*I restriction enzyme binding site near the center of the DNA duplex. Likewise, those 100-mers containing a single CA mismatch also had the mismatch located near the center of the duplex. Well matched 17-mer strands were prepared with the same modifications, the Nile Blue redox probe at one 5′ end and thiol linker at the other 5′ end. The monolayer was assembled on silicon chips bearing sixteen 2 mm^2 gold electrodes that enabled simultaneous comparison of up to four distinct monolayers on a single chip with fourfold redundancy34. All monolayers were assembled as duplex DNA, and prior to testing, the electrodes were backfilled with mercaptohexanol to passivate against direct electrochemistry with the gold surface. The morphology of DNA monolayers on gold electrodes has been previously

investigated with atomic force microscopy37,38; at negative potentials the duplexes are repelled from the surface to a near-vertical orientation.

Electrochemical behavior of well matched and mismatched 100-mer monolayers

First, we explored the general electrochemical characteristics of DNA as a 34 nm molecular bridge between the gold electrode and Nile Blue redox probe. The cyclic voltammetry (CV) from these monolayers is given in Figure 2. The CV from well matched 100-mer monolayers exhibits large peaks associated with the Nile Blue redox probe indicative of effective CT at a midpoint potential of −240 mV versus a Ag/AgCl reference. The integrated cathodic and anodic peak areas for these well matched monolayers are found to be 1.7 ± 0.1 nC and 3.6 ± 0.1 nC, respectively, correlating with a surface coverage of approximately 1 pmol/cm^2; some variations arise with buffer and adventitious oxygen. The surface coverage and the CV peak areas are lower but comparable to those observed with 17-mers. For instance, the average CT through well matched, Nile Blue modified 17-mers is 3.5 ± 0.5 nC, as averaged over 100 electrodes34. Therefore, the 34 nm DNA is comparably effective as a surface-to-probe bridge as smaller oligonucleotides.

To verify that the charge is passing through the DNA, we also measured the electrochemistry of well matched DNA duplexes against duplexes containing a single mismatched base pair (CA) on the same chip (Figure 2a). Mismatched bases have been shown to attenuate DNA CT due to perturbations of the π-stack24,25,34,39. Comparing well matched and mismatched DNA monolayers on the same chip ensures that both are subject to the same processing conditions. As seen, the mismatch clearly attenuates the CT, as the average CV peak area is significantly lower, measuring only 0.8 ± 0.1 nC and 1.8 ± 0.2 nC, for the cathodic and anodic peaks respectively, a factor of two or more lower than the well matched monolayer in each case. The mismatched peaks exhibit slightly larger splitting, though this difference does not hold at higher scan rates. This effect was independent of mismatch position; placement of the mismatch at positions differing by up to 20 base pairs in the 100-mer, through single base changes in the central 36-mer segment, resulted in similar signal attenuation (data not shown). The mismatch inhibits the transport capability of the DNA bridge regardless of its position in the 100-mer.

To establish the reproducibility of mismatch attenuation, we tested DNA CT of well matched and mismatched 100-mer monolayers side-by-side across 6 chips, representing over 40 electrodes of each type of monolayer (configuration as illustrated in Figure 2). It was found that the ratios of the cathodic CV peak areas of well matched to mismatched monolayers were 2.3 ± 0.4. A t-test of this ratio distribution in comparison to the null ratio of 1 has a p-value of 0.0005. By comparison, this well matched to mismatched ratio has been found to be 1.9 to 3.5 for various intercalating redox probes in 15-mer DNA24 and 2.7 to 2.8 for 17-mer DNA with a Nile Blue redox probe34. The consistency of this measured attenuation for mismatches with prior measurements of mismatched monolayers demonstrates that charge flow depends on the integrity of the DNA π-stack, a strong argument that transport is occurring *through* the 100-mer DNA. Furthermore, the fact that a single defect in a 100-mer produces an effect similar to one in much shorter DNA is remarkable given the substantial length disparity.

Kinetics of charge transfer through 100-mer monolayers

Electron transfer kinetics were estimated by measuring the scan rate dependence of the peak splitting between the anodic and cathodic Nile Blue CV peaks of these DNA monolayers. At high scan rates (>1 V/s), the voltammetry enters the totally irreversible reaction regime, and the peak splitting becomes linear with scan rate. By applying Laviron analysis40 in this regime, the electron transfer rate *k* can be estimated. Interestingly, as shown in Figure 3, the

electron transfer kinetics of well matched and mismatched 100-mer DNA monolayers are virtually identical, as with prior measurements of 17-mers34. For the well matched 100-mer, $k_{100} = 39\ s^{-1}$, while the mismatched 100-mer yielded $k_{100} = 40\ s^{-1}$.

Though slow, these transfer rates are significantly faster than that expected for tunneling across 34 nm from the electrode directly to the redox probe41–43. These figures are also indistinguishable (given the analysis) from those obtained from the 17-mer monolayer on the same chip, for which $k_{17} = 25\ s^{-1}$, consistent with our previous studies of DNA of similar lengths34,44–47. Thus, the electron transfer rates of these monolayers exhibit essentially no variation with length over this regime. Previous transfer kinetics studies of DNA monolayers with 16-mer sequences showed an exponential dependence of the electron transfer rate with linker length with a coefficient for the electronic coupling, $\beta = 1\ Å^{-1}$, consistent with values expected for tunneling through a saturated carbon linker47; the extrapolated transfer rate through the 16-mer DNA in the absence of the linker was ~ $10^8\ s^{-1}$. It appears that the rate-limiting step is not CT through the DNA duplex but rather transport through the alkanethiol linker. Thus, the estimated rates are also fully consistent with rapid transfer through the 100-mer DNA assembly.

To provide further evidence that CT in the 100-mer is DNA-mediated and does not involve direct interaction of the Nile Blue probe with the surface, we prepared a chip with the well matched 100-mer, a well matched 17-mer, the 100-mer assembly missing the central 36-mer single stranded segment and the single stranded 25-mer DNA modified with the Nile Blue probe alone without complement (Figure 4). The single stranded 25-mer modified with Nile Blue provides a clear control for direct contact of the redox probe with the surface. Here the 25-mer, lacking a thiol, is adsorbed onto the gold through direct interactions of the bases and redox probe with the surface; the probe reduction is not DNA-mediated. Consistent with this, it is evident in Figure 4 that the CV of the 100-mer differs significantly from that of the adsorbed single stranded DNA modified with Nile Blue, not only with respect to the signal intensity and peak shape but also with respect to peak splitting and midpoint potential. The CV of the 100-mer instead resembles that of the 17-mer, where CT is DNA-mediated. Moreover, while direct surface reduction of the Nile Blue probe on the single stranded DNA yields a sharp CV peak that shows only minor splitting at fast scan rates, DNA-mediated reduction of the Nile Blue probe through the well matched 100-mer and 17-mer yields a broad peak that is significantly split and further broadened at fast scan rates. These pronounced visible differences in the electrochemistry can be attributed to the greater kinetic barrier associated with charge transfer *through* the DNA as compared to direct contact and reduction at the electrode surface. This kinetic difference is further highlighted by the measured CT rates for these samples; surface reduction of the Nile Blue probe on single stranded DNA occurs at a nearly 40-fold faster rate than charge transfer through the 100-mer and 17-mer DNA, based on Laviron analysis for these chips. It should be noted that while kinetic comparisons can be made among these assemblies, signal intensities are hard to compare because of the substantial differences in mode of adherence to the surface and the resultant packing densities.

As evident in Figure 4, leaving out the central 36-mer to create a duplex with a central single stranded segment that can easily bend and sway also yields drastic electrochemical changes. Not only is its redox peak significantly smaller than the fully assembled 100-mer (cathodic peak size of 0.7 nC vs. 2 nC for each, respectively), the decreased peak splitting, and sharper peak shape much more closely resemble those of the single stranded Nile Blue-modified DNA sample. Thus the Nile Blue redox signal of the 100-mer DNA missing the 36-mer segment is likely due to direct contact of the probe with the surface just as for the single-stranded 25-mer. Interestingly, the signal for this disordered jumble of DNA on the surface

is much smaller than the signal from either the single stranded Nile Blue-modified DNA or the fully assembled, well-matched 100-mer.

Restriction Enzyme activity on 100-mer monolayers

Restriction enzyme activity with these 100-mer-modified electrodes provides another probe of the DNA-mediated reaction. To facilitate restriction, the restriction site must be accessible for protein binding and in a biologically recognizable conformation. If the restriction site is below the Nile Blue redox probe and if the duplex is upright and not contacting the surface, successful cutting will release the probe into solution. This activity would destroy the DNA-mediated CT pathway to the probe to yield significant loss of the redox signal.

To test for restriction enzyme activity, the chip setup shown in Figure 4 was exposed to the restriction enzyme *Rsa*I which cuts the sequence 5′-GTAC-3′ with high specificity and leaves blunt ends on the resulting DNA segments. After incubation of the enzyme with 10 mM Mg^{2+} for 15 minutes on the chip, signal attenuation (90% by the cathodic peak area of the CV) is observed for the 100-mer while the other quadrants remain essentially unchanged. This result clearly demonstrates that the DNA in these 100-mer monolayers is accessible to the protein and in a biologically relevant conformation. Moreover in the 100-mer, CT is necessarily DNA-mediated. For the quadrant containing the single stranded Nile Blue probe which is in direct contact with the surface, exposure to *Rsa*I causes no change in the signal. For the quadrant containing the 100-mer missing the central 36-mer segment, the minimal signal loss (10% by the cathodic peak of the CV) is likely due to the instability of this assembly to the electrode rinsing and buffer exchange steps required for this experiment. For the 17-mer duplex, there is no restriction site and therefore no expectation of signal attenuation. For the 100-mer, then, the attenuation we observe must reflect that CT to the Nile Blue probe is DNA-mediated.

Restriction enzyme activity was also monitored as a function of time in the well matched 100-mer alongside other DNA duplexes containing the *Rsa*I binding site including a new well matched 17-mer and the 100-mer with a single base pair mismatch (not at the restriction site). As these three types of DNA all contain the *Rsa*I binding site, successful cutting will result in detachment of the Nile Blue redox probe and attenuation of the electrochemical signal. As a negative control, one well of the chip was modified with the well matched 100-mer but kept free of *Rsa*I. Figure 5 illustrates the activity of *Rsa*I over time on these DNA samples. Initially, before the enzyme is added, the signals from all monolayers are stable in the buffer solution. Subsequently *Rsa*I is added to the quadrants containing the well matched 100-mer, well matched 17-mer, and mismatched 100-mer. The fourth quadrant, which was modified with the well matched 100-mer, was isolated in a separate well that was maintained free of enzyme. Activation of the enzyme with Mg^{2+} triggers a rapid decrease in integrated charge from the *Rsa*I-exposed quadrants, while the signal from the quadrant without enzyme increases slightly. The loss of Nile Blue signal for the three connected quadrants is consistent with *Rsa*I cleavage activated by divalent cations; Mg^{2+} apparently enhances the signal from the isolated quadrant. The observation of enzymatic activity in these monolayers demonstrates that the DNA is in its native conformation and biologically active.

DISCUSSION

DNA-mediated electrochemistry through 100-mer monolayers reveals large signals for well matched duplexes, comparable to what is observed with shorter duplexes. This result indicates that CT through DNA is robust in these long DNA films. Nonetheless, attenuation by single base mismatches speaks to the delicacy of this process and strongly argues that the

integrity of the base pair π-stack is crucial. The fact that a single mismatch within a 100-mer of otherwise well matched bases causes signal attenuation equal to that seen in mismatched DNA ~20% the length establishes a new point of reference for the sensitivity of DNA CT to minor perturbations. Cutting with the *Rsa*I restriction endonuclease demonstrates the biological integrity of the monolayers and also illustrates the utility of these longer DNA assemblies for sensing of DNA-binding protein reactions. The ability to construct these CT-active assemblies using smaller oligonucleotides may be particularly useful for associated nanoelectronics applications. All of these results document that DNA can efficiently facilitate charge transport over 100 base pairs, or 34 nm, close to the persistence length of duplex DNA in solution. This is a remarkable distance for CT, surpassing other reports of long range transport through conjugated molecular wires[8,9], and is among the longest distances reported for a molecular monolayer[4,5,7,48].

From our estimates of electron transfer rates, which are essentially the same for the 100-mer and 17-mer, the rate-limiting step must still be tunneling through the alkanethiol linker. This puts a lower bound on the rate of electron transfer through the 100-mer DNA itself. In our earlier studies of a 16-mer, where we saw significant variations in rate due to linker length, we could extrapolate that the rate of electron transfer through the 16-mer must be $>10^8$ s^{-1}. Given our lower bound for the 100-mer, $k_{100} = 10^2$ s^{-1}, i.e. no faster than that through the linker, we obtain an estimate for β of 0.05 $Å^{-1}$ through the DNA. This conservative estimate is in the range of conventional conjugated molecular wires[2–9] (0.001 to 0.2 $Å^{-1}$). Simply put, even for this 34 nm DNA wire, the small alkane thiol linker is still rate-limiting.

The full mechanism associated with this DNA-mediated electrochemistry is still elusive, and this study highlights several observations that are difficult to reconcile. A variety of redox probes, covering reduction potentials ranging over nearly a volt, are compatible with DNA electrochemistry as long as the probes are electronically well coupled to the DNA base pair stack[28]. We find for all of these probes that they are reduced near their free redox potentials. However, the reduction potentials of the individual bases are all significantly higher than the redox potentials of the probes. In this study, the reduction potential of Nile Blue (−250 mV vs. Ag/AgCl) is substantially more positive than any of the free bases (<−1V vs. Ag/AgCl)[49]. To date, direct reduction of DNA has not been observed at the potentials of these redox probes, nor would it be consistent with the parameters involved. This conundrum could be reconciled if the stacked DNA duplex forms a delocalized band structure, different from individual bases, having a low-lying LUMO from the overlapping π-orbitals of the bases. While such a band structure is plausible, an equilibrium band structure has not to date been observed experimentally. Our group has thus postulated that DNA CT is conformationally gated, and that the CT-active state or states are transient, nonequilibrium states[50]. Experimental evidence suggests that in solution these states, what we consider to be delocalized domains of the π-stacked bases, extend over ~ 4 base pairs[50]. Whether these domains are more extended or less transient within the DNA film versus in solution is unclear. Unlike conventional molecular wires, which exhibit inherent rigidity, DNA is undergoing motions on the ps to ms time scales. The fleeting alignment of the bases creates a delicate π-network with CT states that are only transiently active. The observation that a single mismatch in a 100-mer is resolved with the same degree of signal attenuation as seen in much shorter DNA further underscores how remarkably small perturbations in this system profoundly influence the global orbital network. A poorly stacked single base pair mismatch may block formation of potential band structure.

Is DNA a molecular wire? In this experiment, it can clearly bridge the electrode and redox probe over 34 nm. DNA not only fulfills many of the requirements of molecular wires but surpasses conventional wires in its ease of synthesis and flexibility of design. However, this is a transient and fragile wire, as it must be maintained in buffered solution, and effective

conduction over its length is extraordinarily sensitive to subtle structural variations. Indeed, the DNA bridge may be considered instead an extension of the gold electrode, a 34 nm-long sensor to detect solution-borne targets. While the sensitivity to base stacking presents a challenge to use DNA as a molecular wire for integrated circuits, the ability to make long, well coupled DNA assemblies in circuits is a clear benefit. Moreover, the DNA wire is ideal for biosensing under physiological conditions.

Methods

Oligonucleotide synthesis and purification

Oligonucleotides were synthesized on an Applied Biosystems 3400 DNA synthesizer. Each double stranded 100-mer was formed from five single stranded segments (see Supporting Information Figure 1) that were annealed to form the complete sequence 5′-(SH linker)-AGT ACT GCA GTA GCG ACG TCA TAG GAC ATC AGT CTG CGC CAT TCA TGA CAT AC*G TAC* GCA GTA GGT GAA **A** TCG TGG CAG GTC AGT CAT GTA TAC TGC ACT A-3′ with the complementary sequence containing a Nile Blue redox probe coupled through a 5′ terminal uracil analog, as described previously33,35. For the mismatched 100-mer duplex, a single base pair mismatch (CA) was incorporated primarily at **A**, experiemnts were also carried out for comparison with mismatches generated at the underlined bases; the italicized bases 5′-*GTAC*-3′ mark the location of the *Rsa*I binding site. The linker was the six-carbon thiol modifier C6 S-S from Glen Research. The 17-mer duplexes were prepared with the sequences 5′-(SH linker)-GA GAT ATA AAG CAC GCA -3′ for the 17-mer without the *Rsa*I binding site and 5′-(SH linker)-GA GAT ATA AA*G TAC* GCA-3′ for the 17-mer with the *Rsa*I binding site with the respective, complementary well matched Nile Blue-modified single strand for each. Each single strand was purified by HPLC using a 50 mM ammonium acetate buffer/acetonitrile gradient. The synthesis and purification of each strand, including Nile Blue and C6 thiol modification, followed the reported protocol33. For the 73-mer strand, the HPLC column was heated to 40 °C to discourage formation of secondary structure. The purified oligonucleotides were subsequently desalted and quantified by UV-visible spectrophotometry according to their extinction coefficients (IDT Oligo Analyzer). Duplexes were formed by thermally annealing equimolar amounts of oligonucleotides at 90 °C for 5 min in deoxygenated phosphate buffer (5 mM NaPhos, 50 mM NaCl, pH 7.0) followed by slow cooling to ambient temperature. The integrity of each strand was verified by HPLC, MALDI-TOF mass spectrometry and UV-Vis spectroscopy, and full hybridization and stoichiometry of double stranded DNA solutions were confirmed through UV melting temperature analysis (See Supporting Information Figure 2).

Preparation of DNA monolayers and electrochemical analysis

DNA monolayers were formed by assembly on chips bearing 16 gold electrodes that have been described previously14. Each chip was prepared with up to four sequences of 25 μM duplex DNA solutions in phosphate buffer containing 100 mM $MgCl_2$. Monolayer formation was typically allowed to proceed in a humidified environment for a period of 16–20 h. Upon completion of film formation, the cell was backfilled with 0.5 mM 1-mercaptohexanol in a 95:5 phosphate buffer/glycerol solution for 60 min. The electrodes were rinsed thoroughly prior to electrochemistry experiments to ensure removal of residual alkanethiols. Cyclic voltammetry and square wave voltammetry experiments were performed by automated measurement with a CH760B Electrochemical Analyzer and a 16-channel multiplexer module from CH Instruments (Austin, TX). Chips were tested with a common Pt auxiliary electrode and a common Ag/AgCl reference electrode. Unless otherwise noted, electrochemistry was recorded at ambient temperature in Tris buffer containing 10 mM Tris, 50 mM NaCl, 10 mM $MgCl_2$, and 4 mM spermidine at pH 7.1. Electron transfer kinetics were estimated by Laviron analysis40.

Restriction assay

The restriction enzyme *Rsa*I was purchased from New England Biolabs. The shipping buffer was exchanged to Tris buffer containing 10 mM Tris, 50 mM NaCl and 4 mM spermidine, pH 8.0, using a Pierce Slide-A-Lyzer minidialysis kit with overnight stirring. Measurements were executed on chips with the standard, single well setup as well as with a custom well clamp bearing a control quadrant to maintain one quadrant free of enzyme (see Supporting Information Figure 3). The reference and counter electrodes were thoroughly rinsed with deionized water when transferring between wells.

Supplementary Material

Refer to Web version on PubMed Central for supplementary material.

Acknowledgments

This research was supported by the NIH (GM61077). J.D.S. also thanks the National Institute of Biomedical Imaging and Bioengineering for a postdoctoral fellowship (F32EB007900). The authors thank J. Genereux, A. Gorodetsky and M. Buzzeo for fruitful discussions, and Kevin Kan for assistance with fabrication of the silicon chips. This work was completed in part in the Caltech Micro Nano Fabrication Laboratory.

References

1. Robertson N, McGowan CA. A comparison of potential molecular wires as components for molecular electronics. Chem Soc Rev. 2003; 32:96–103. [PubMed: 12683106]
2. Chen F, Tao NJ. Electron Transport in Single Molecules: From Benzene to Graphene. Acc Chem Res. 2009; 42:429–438. [PubMed: 19253984]
3. Malliaras G, Friend R. An Organic Electronics Primer. Phys Today. 2005; 58(5):53–58.
4. Tuccitto N, et al. Highly conductive ~40-nm-long molecular wires assembled by stepwise incorporation of metal centres. Nat Mater. 2009; 8:41–46. [PubMed: 19011616]
5. Choi SH, Kim B, Frisbie CD. Electrical Resistance of Long Conjugated Molecular Wires. Science. 2008; 320:1482–1486. [PubMed: 18556556]
6. Liu L, Frisbie CD. Length-Dependent Conductance of Conjugated Molecular Wires Synthesized by Stepwise "Click" Chemistry. J Am Chem Soc. 2010; 132:8854–8855. [PubMed: 20550115]
7. Søndergaard R, et al. Conjugated 12 nm long oligomers as molecular wires in nanoelectronics. J Mater Chem. 2009; 19:3899–3908.
8. Hu W, et al. Electron Transport in Self-Assembled Polymer Molecular Junctions. Phys Rev Lett. 2006; 96:027801. [PubMed: 16486641]
9. Vura-Weis J, et al. Crossover from Single-Step Tunneling to Multistep Hopping for Molecular Triplet Energy Transfer. Science. 2010; 328:1547–1550. [PubMed: 20558715]
10. Drummond TG, Hill MG, Barton JK. Electrochemical DNA Sensors. Nat Biotechnol. 2003; 21:1192–1199. [PubMed: 14520405]
11. Liu J, Cao Z, Lu Y. Functional Nucleic Acid Sensors. Chem Rev. 2009; 109:1948–1998. [PubMed: 19301873]
12. Endres RG, Cox DL, Singh RRP. Colloquium: The quest for high-conductance DNA. Rev Mod Phys. 2004; 76:195–214.
13. Roy S, et al. Direct Electrical Measurements on Single-Molecule Genomic DNA Using Single-Walled Carbon Nanotubes. Nano Lett. 2008; 8:26–30. [PubMed: 18052084]
14. Murphy CJ, et al. Long-Range Photoinduced Electron Transfer Through a DNA Helix. Science. 1993; 262:1025–1029. [PubMed: 7802858]
15. Fink HW, Schoenberger C. Electrical conduction through DNA molecules. Nature. 1999; 398:407–410. [PubMed: 10201370]
16. de Pablo PJ, et al. Absence of dc-Conductivity in λ-DNA. Phys Rev Lett. 2000; 85:4992–4995. [PubMed: 11102169]

17. Kasumov, AYu, et al. Proximity-Induced Superconductivity in DNA. Science. 2001; 291:280–282. [PubMed: 11209072]
18. Storm AJ, van Noort J, de Vries S, Dekker C. Insulating behavior for DNA molecules between nanoelectrodes at the 100 nm length scale. Appl Phys Lett. 2001; 79:3881–3883.
19. Guo X, Gorodetsky AA, Hone J, Barton JK, Nuckolls C. Conductivity of a single DNA duplex bridging a carbon nanotube gap. Nature Nanotech. 2008; 3:163–167.
20. Kelley SO, Barton JK. Electron Transfer Between Bases in Double Helical DNA. Science. 1999; 283:375–381. [PubMed: 9888851]
21. Cohen H, Nogues C, Naaman R, Porath D. Direct measurement of electrical transport through single DNA molecules of complex sequence. Proc Natl Acad Sci USA. 2005; 102:11589–11593. [PubMed: 16087871]
22. Xu B, Zhang P, Li X, Tao N. Direct Conductance Measurement of Single DNA Molecules in Aqueous Solution. Nano Lett. 2004; 4:1105–1108.
23. Kelley SO, Holmlin RE, Stemp EDA, Barton JK. Photoinduced Electron Transfer in Ethidium-Modified DNA Duplexes: Dependence on Distance and Base Stacking. J Am Chem Soc. 1997; 119:9861–9870.
24. Kelley SO, Boon EM, Barton JK, Jackson NM, Hill MG. Single-base mismatch detection based on charge transduction through DNA. Nucleic Acids Res. 1999; 27:4830–4837. [PubMed: 10572185]
25. Boon EM, Ceres DM, Drummond TG, Hill MG, Barton JK. Mutation detection by electrocatalysis at DNA-modified electrodes. Nat Biotechnol. 2000; 18:1096–1100. [PubMed: 11017050]
26. Núñez ME, Hall DB, Barton JK. Long-range oxidative damage to DNA: effects of distance and sequence. Chem Biol. 1999; 6:85–97. [PubMed: 10021416]
27. Boon EM, Salas JE, Barton JK. An electrical probe of protein-DNA interactions on DNA-modified surfaces. Nat Biotechnol. 2002; 20:282–286. [PubMed: 11875430]
28. Genereux JC, Barton JK. Mechanisms for DNA Charge Transport. Chem Rev. 2010; 110:1642–1662. [PubMed: 20214403]
29. Wagenknecht, H-A. Charge transfer in DNA: from mechanism to application. Wiley VCH; Weinheim, Germany: 2005.
30. Kawai K, Kodera H, Osakada Y, Majima T. Sequence-independent and rapid long-range charge transfer through DNA. Nature Chem. 2009; 1:156–159. [PubMed: 21378829]
31. Douglas SM, et al. Self-assembly of DNA into nanoscale three-dimensional shapes. Nature. 2009; 459:414–418. [PubMed: 19458720]
32. Rothemund PWK. Folding DNA to create nanoscale shapes and patterns. Nature. 2006; 440:297–302. [PubMed: 16541064]
33. Soleymani L, et al. Programming the detection limits of biosensors through controlled nanostructuring. Nature Nanotechnology. 2010; 4:844–848.
34. Slinker JD, Muren NB, Gorodetsky AA, Barton JK. Multiplexed DNA-Modified Electrodes. J Am Chem Soc. 2010; 132:2769–2774. [PubMed: 20131780]
35. Liu T, Barton JK. DNA Electrochemistry through the Base Pairs Not the Sugar-Phosphate Backbone. J Am Chem Soc. 2005; 127:10160–10161. [PubMed: 16028914]
36. Gorodetsky AA, Ebrahim A, Barton JK. Electrical Detection of TATA Binding Protein at DNA-Modified Microelectrodes. J Am Chem Soc. 2008; 130:2924–2925. [PubMed: 18271589]
37. Kelley SO, et al. Orienting DNA Helices on Gold Using Applied Electric Fields. Langmuir. 1998; 14:6781–6784.
38. Sam M, Boon EM, Barton JK, Hill MG, Spain EM. Morphology of 15-mer Duplexes Tethered to Au(111) Probed Using Scanning Probe Microscopy. Langmuir. 2001; 17:5727–5730.
39. Boal AK, Barton JK. Electrochemical Detection of Lesions in DNA. Bioconjugate Chem. 2005; 16:312–321.
40. Laviron E. General expression of the linear potential sweep voltammagram in the case of diffusionless electrochemical systems. J Electroanal Chem. 1979; 101:19–28.
41. Weber K, Hockett L, Creager S. Long-Range Electronic Coupling between Ferrocene and Gold in Alkanethiolate-based Monolayers on Electrodes. J Phys Chem B. 1997; 101:8286–8291.

42. Huang K, et al. Ferrocene and Porphyrin Monolayers on Si(100) Surfaces: Preparation and Effect of Linker Length on Electron Transfer. ChemPhysChem. 2009; 10:963–971. [PubMed: 19263452]
43. Yu HZ, Shao HB, Luo Y, Zhang HL, Liu ZF. Evaluation of the Tunneling Constant for Long Range Electron Transfer in Azobenzene Self-Assembled Monolayers on Gold. Langmuir. 1997; 13:5774–5778.
44. Boon EM, Barton JK. Reduction of Ferricyanide by Methylene Blue at a DNA-Modified Rotating-Disk Electrode. Langmuir. 2003; 19:9255–9259.
45. Kelley SO, Jackson NM, Hill MG, Barton JK. Long-Range Electron Transfer through DNA Films. Angew Chem, Int Ed. 1999; 38:941–945.
46. Gorodetsky AA, Green O, Yavin E, Barton JK. Coupling into the Base Pair Stack Is Necessary for DNA-Mediated Electrochemistry. Bioconjugate Chem. 2007; 18:1434–1441.
47. Drummond TG, Hill MG, Barton JK. Electron Transfer Rates in DNA Films as a Function of Tether Length. J Am Chem Soc. 2004; 126:15010–15011. [PubMed: 15547981]
48. Arikuma Y, Nakayama H, Morita T, Kimura S. Electron Hopping over 100 Å along an α Helix. Angew Chem Int Ed. 2010; 49:1800–1804.
49. Steenken S, Telo JP, Novais HM, Candeias LP. One-electron-reduction potentials of pyrimidine bases, nucleosides, and nucleotides in aqueous solution. Consequences for DNA redox chemistry. J Am Chem Soc. 1992; 114:4701–4709.
50. Genereux JC, Augustyn KE, Davis ML, Shao F, Barton JK. Back-Electron Transfer Suppresses the Periodic Length Dependence of DNA-Mediated Charge Transport across Adenine Tracts. J Am Chem Soc. 2008; 130:15150–15156. [PubMed: 18855390]

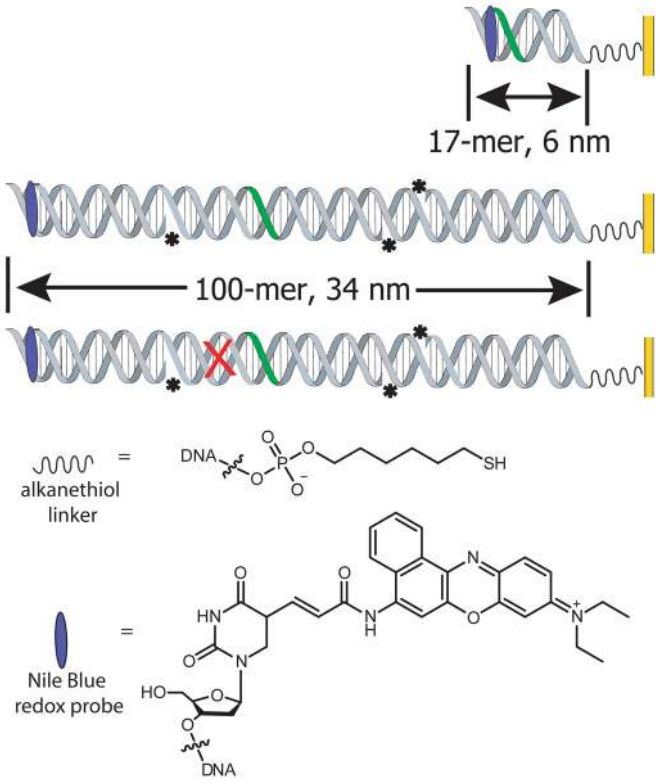

Figure 1.

Illustration of the DNAs used on the electrodes. Shown are (top to bottom) a well matched 17-mer; a well matched 100-mer; a 100-mer with a single mismatched base pair; the six carbon alkanethiol linker; and the Nile Blue redox probe coupled through a uracil. The green sections of the 100-mer mark the approximate location of the *Rsa*I restriction enzyme binding site, and the X notes the approximate location of the single CA mismatch, 69 bases from the thiolated end of the duplex. The asterisks on the sugar phosphate backbone of the 100-mers indicate the location of nicks. The specific sequences are noted in the methods.

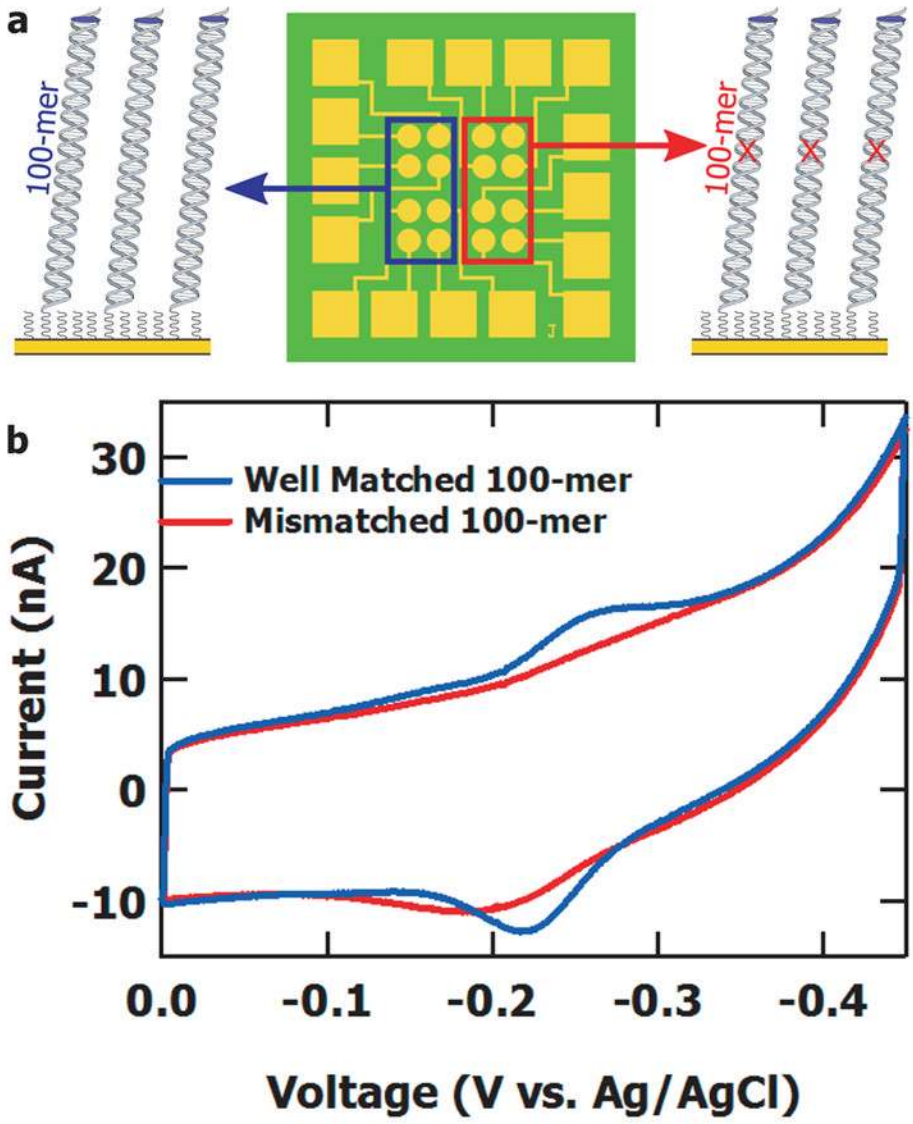

Figure 2.

Electrochemistry from 100-mer well matched and mismatched monolayers. **a**, Illustration of the chip layout for comparing monolayer electrochemistry between well matched 100-mers and 100-mers with a single base pair mismatch. A mismatch (CA) is generated in the 36-mer segment by substitution of a C for a T at the position 69 bases from the thiolated end of the duplex. **b**, Average cyclic voltammetry curves from well matched (blue) and mismatched (red) 100-mer DNA, each modified with a Nile Blue redox probe. Data were obtained at a 50 mV/s scan rate in Tris buffer (10 mM Tris-HCl, 50 mM NaCl, 10 mM $MgCl_2$ and 4 mM spermidine, pH 7) and averaged over the similar electrodes on each chip.

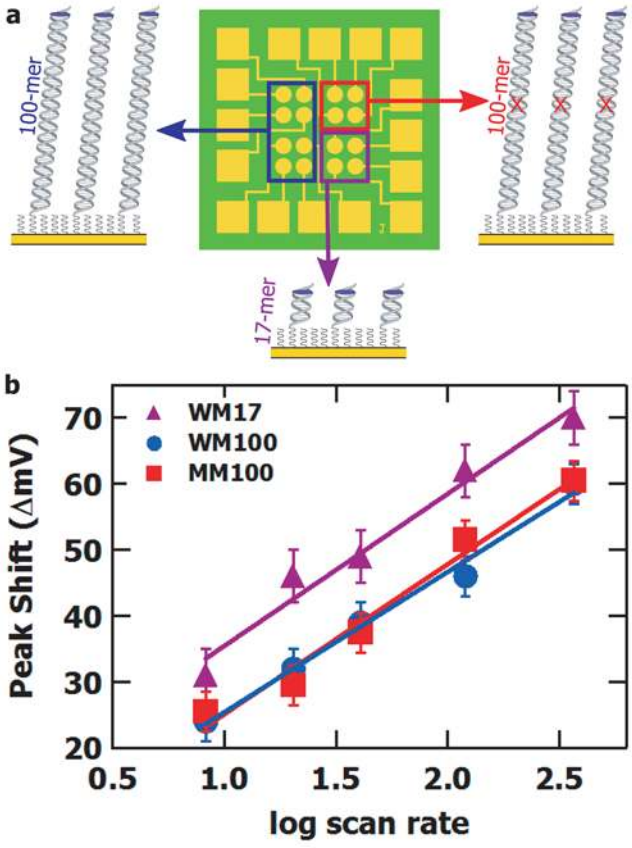

Figure 3.

Kinetics of CT through 100-mer and 17-mer monolayers**. a**, Illustration of the chip layout for testing electron transfer kinetics. **b**, Cyclic voltammetry peak splitting versus scan rate for well matched and mismatched 100-mer DNA monolayers along with well matched 17-mer monolayers as averaged over four devices on a single chip. Data were obtained in 10 mM Tris-HCl, 50 mM NaCl, 10 mM $MgCl_2$ and 4 mM spermidine, pH 7. By applying Laviron analysis in this linear regime, the electron transfer coefficient and electron transfer rate were extracted. Values are $\alpha = 0.6$ and $k = 30–40\ s^{-1}$ for well matched 100-mer, mismatched 100-mer, and well matched 17-mer monolayers.

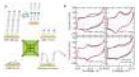

Figure 4.

Electrochemistry and enzymatic activity on various DNA films. **a**, Illustration of the chip layout for measuring the electrochemical characteristics and *Rsa*I activity with four DNA films (from top left to bottom right) including the well matched 100-mer which contains the *Rsa*I binding site, a well matched 17-mer that does not contain the *Rsa*I binding site, the single stranded, Nile Blue modified 25-mer, and the 100-mer missing the central 36-mer segment. As illustrated, the 25-mer and 100-mer without the central 36-mer are expected to be reduced through direct surface adsorption and contact. In **a** is also illustrated restriction of the well matched 100-mer DNA films upon addition of *Rsa*I and Mg^{2+}. **b**, CV scans of the four DNA films prior to addition of enzyme (blue) and after addition of *Rsa*I (red). The enzyme reaction was carried out in 10 mM tris-HCl, 50 mM NaCl, 10 mM $MgCl_2$, 4 mM spermidine, pH 7.9. Scans were taken before and after the enzyme reaction in phosphate buffer (5 mM phosphate, 50 mM NaCl, 4 mM $MgCl_2$, 4 mM spermidine, 10% glycerol, pH 7). CV scans were measured versus Ag/AgCL at a 100 mV/s scan rate. For the 100-mer, 17-mer and single stranded 25-mer, respectively, the peak splittings are 80 mV, 60 mV, and 15mV; the midpoint potentials are −180 mV, −180mV, and −170mV; $k_{100} = k_{17} = 39\ k_{ss25}$. Values could not be determined accurately for the 100-mer lacking the 36-mer strand.

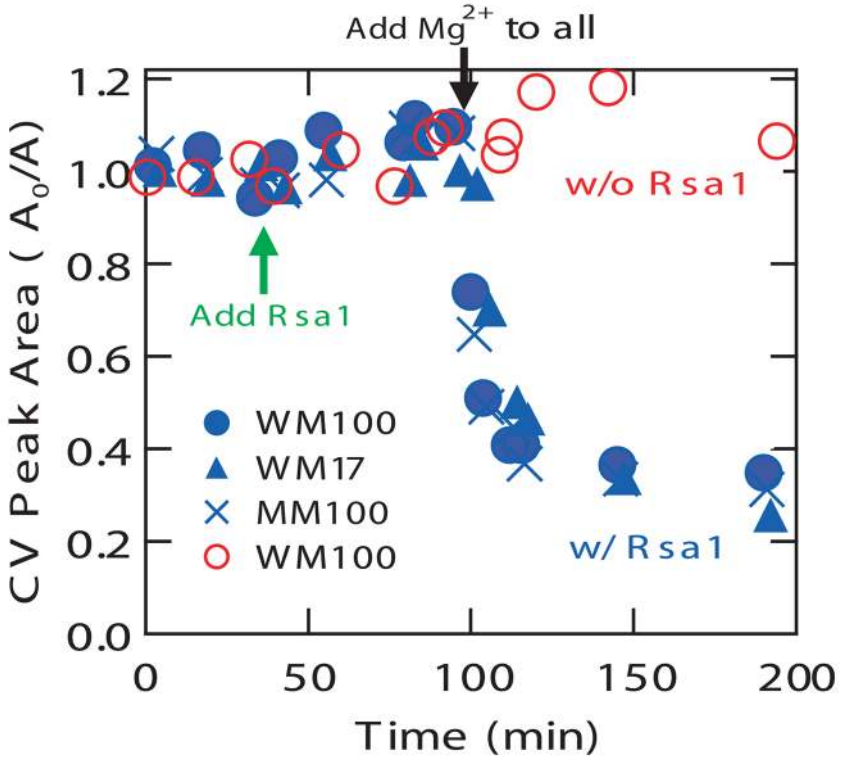

Figure 5.

Enzymatic activity on 100-mer monolayers as a function of time. Integrated cathodic CV peak area versus time for various DNA monolayers exposed to *Rsa*I (blue) and 100-mer DNA in the absence of enzyme (red). The types of DNA tested include the well matched 100-mer, a well matched 17-mer, and the mismatched 100-mer, all of which contain the *Rsa*I binding site. The charge was obtained by integrating the cathodic Nile Blue CV peaks obtained at a 100 mV/s scan rate.